Reflections inside an elliptical dielectric lens antenna

A. Neto
S. Maci
P.J.I. de Maagt

Indexing terms: Dielectric lens antenna, Elliptical lens, Reflections, Radiating element, Input impedance, Caustic

Abstract: The reflections inside the elliptical lens of a typical millimetre wave antenna are investigated. In particular, it is seen that these reflections may significantly affect the input impedance of a radiating element which is located at the lens focus, owing to the presence there of a point caustic of doubly reflected rays. The presence of a caustic prevents the field prediction inside the lens by a direct application of geometrical optics. Consequently, the field inside the lens is calculated by means of the physical optics currents associated with singly and doubly reflected rays.

1 Introduction

Planar radiating elements covered by dielectric lenses have the potentiality to be used as antennas for millimetre and submillimetre wave receivers [1–5]. The wide attention they have been receiving recently is due to their capability to be integrated with electronic components such as detecting diodes, local oscillators and mixers. Furthermore, they provide a good efficiency with respect to other millimetre wave antennas printed on homogeneous substrates, essentially because they do not suffer from loss of power in guided modes. The elliptical shape of the lens gives high focusing properties provided that its eccentricity is properly related to its dielectric constant. On the other hand the lens interface gives rise to reflections inside the lens, that may significantly affect the input impedance and the radiation properties. This aspect, which has not been properly investigated in the literature, is a critical point in the overall design of lens antennas, and it is the main topic of this paper. The geometrical properties of the lens itself are such that all the doubly reflected rays launched by a focal source return at the original focus. This means that a point caustic of doubly reflected rays occurs exactly where the primary feed source is located. In order to limit these reflections, a quarter wavelength matching layer can be used [5]. However, in practice the manufacturing of a matching layer is not straightforward. Furthermore, the availability of CAD tools for predicting accurately the input impedance of the antenna (including multiple reflections effects) is particularly important owing to the limited tuning possibilities intrinsic with integrated technology.

IEE Proceedings online no. 19981884

Paper first received 27th June 1997 and in revised form 5th January 1998

A. Neto and S. Maci are with the College of Engineering, University of Siena, Via Roma 56, 53100, Siena, Italy

P.J.I. de Maagt is with the Antenna Section, Electromagnetic Division, ESA-ESTEC, 2200 AG Noordwijk, The Netherland

2 Ray description

The geometry of the antenna is shown in Fig. 1. A resonating slot antenna on a ground plane is located at the lower focus of a dielectric elliptical lens with permittivity ε_{r1}. A rectangular reference system (x, y, z) is introduced, with the origin at the lower focus, the z axis normal to the ground plane, and the x axis parallel to the slot. The lens has its major semiaxis along z and it is rotationally symmetric. An infinite dielectric medium with constant ε_{r2} is supposed to be below the ground plane. For the sake of simplicity, the slot can be thought of as fed by an impressed voltage at its centre. When the eccentricity e of the ellipse is related to the lens dielectric constant by $e = 1/\sqrt{\varepsilon_r}$ all the rays outgoing from the focal source that impinge on the lens interface above the section BB′ (Fig. 1), are refracted in the z direction [1]. This constructs on a plane $z = const.$, an aperture which is illuminated by in phase ray-field contributions, thus providing high directivity in the z direction. The primary rays incident exactly at the section BB′ are associated with critical angles of incidence. The primary rays that impinge below BB′ are not refracted in the z direction and give rise to a nonfocused radiation that creates spillover of power.

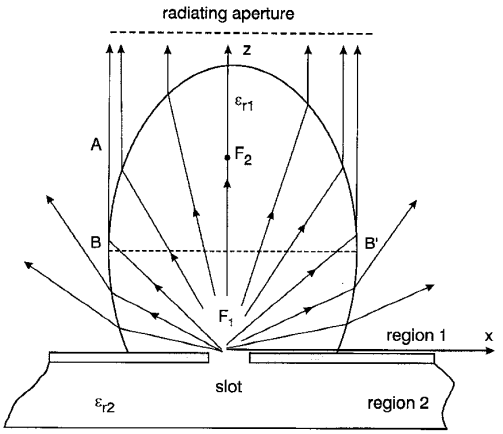

Fig. 1 *Geometry of the lens antenna and ray construction of the aperture field*

Let us consider now the reflection inside the lens (Fig. 2*a*). The rays emanating from the point source F_1,

after reflecting at the interface, pass through the upper focus F_2 of the ellipse, which is a point caustic of singly reflected rays. After that the rays undergo another reflection at the lens interface and then return to the original focus. This focus, where the source is located, is then a point caustic of doubly reflected rays. For the present grounded geometry, not all the rays return at the original source after two reflections. Indeed, rays launched by the source inside the solid angle Ω subtended by the surface A_Ω (Fig. 2*b*), have the second reflection on the ground plane. After this, the rays are not focused at F_1, but have multiple reflections that provide an incoherent superposition of field contributions at the focal point. Consequently the contribution of these rays can be neglected in calculating the input impedance of the slot. To predict the field at F_1 one cannot directly apply geometrical optics (GO) due to the occurrence of the point caustic. On the other hand, the GO can be used to define physical optics (PO) currents of the first and second reflection, as is done in the following Section.

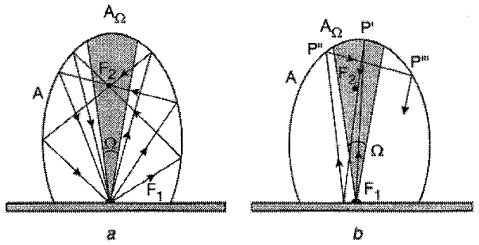

Fig. 2 *Reflection mechanisms inside the lens*
(a) Paths of the rays doubly reflected on the lens surface and shadow angle (Ω)
(b) Multiple reflections of rays launched inside the shadow angle

3 PO currents at the lens surface

By applying the equivalence principle, the slot is substituted by a metallic plug with two magnetic current distributions $\pm \vec{m}(x, y)$ below and above the ground plane, which have the same amplitude but opposite sign to ensure continuity of the tangential electric field component across the slot; this allows one to divide the space into two regions in which the field can be calculated separately. In the following we will focus on prediction of the field in the upper region (region 1 in Fig. 1).

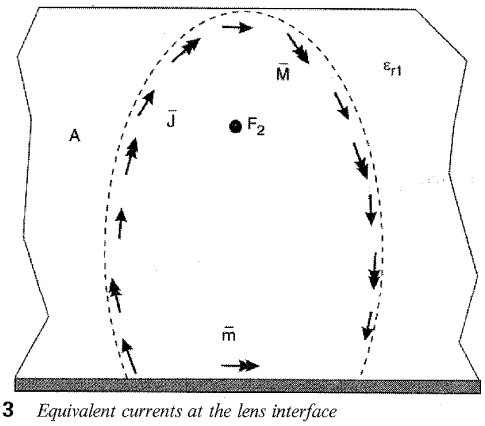

Fig. 3 *Equivalent currents at the lens interface*

Let us first focus on the field inside the lens. By applying the equivalence principle to the surface A of the lens, with normal $\hat{n}$ defined toward the dielectric, electric $\vec{J}$ and magnetic $\vec{M}$ equivalent currents at each point P on A are defined by means of the total tangential field. As depicted in Fig. 3 the region external to A is filled with the same dielectric as that of the lens, so that the radiation of these currents can be obtained by using the Green's function of a homogeneous medium.

3.1 Currents associated with singly reflected rays

Owing to the large radius of curvature of the lens in terms of wavelength, the current distributions can be estimated by the PO approximation

$$\vec{J}^{PO'} = \vec{J}^{PO'}_{inc} + \vec{J}^{PO'}_{ref} = \hat{n} \times \vec{H}^{inc} + \hat{n} \times \underline{\Gamma}^{h} \cdot \vec{H}^{inc} \quad (1)$$

$$\vec{M}^{PO'} = \vec{M}^{PO'}_{inc} + \vec{M}^{PO'}_{ref} = -\hat{n} \times \vec{E}^{inc} - \hat{n} \times \underline{\Gamma}^{e} \cdot \vec{E}^{inc} \quad (2)$$

where $(\vec{E}^{inc}, \vec{H}^{inc})$ is the field incident from the source, and $\underline{\Gamma}^{e,h}$ are the pertinent reflection dyadics of the lens–air interface. For continuity of the tangential field components, the same currents, but with opposite signs, predict the field outside the lens when radiating in a grounded free-space.

In eqns. 1 and 2, two contributions have been defined that are associated to the incident and to the reflected field. The current associated with the incident field provides exactly a zero field inside the lens when integrated on the surface A. To demonstrate this statement, let us suppose that the source $\vec{m}$ radiates in a homogeneous medium with dielectric constant ε_{r1}. Furthermore, apply the equivalence principle to the same surface A as before, but with reverse normal. In such a case, the electric and magnetic currents defined on it are exactly $(-\vec{J}^{PO'}_{inc}, -\vec{M}^{PO'}_{inc})$, where the minus sign is due to the change in direction of the normal. These currents, radiating in the homogeneous medium, provide by definition the incident field of the source outside A and a zero field inside A; thus, demonstrating the assertion, apart from an insignificant change of sign. Consequently, in order to calculate the field inside the lens, only the contribution $(\vec{J}^{PO'}_{ref}, \vec{M}^{PO'}_{ref})$ has to be retained in eqn. 2. Obviously, to predict the field outside the lens, both contributions in eqn. 2 must be considered.

3.2 Currents associated with doubly reflected rays

The ordinary PO method described above does not account for multiple reflections inside the lens, which provide currents on A whose radiating contributions could combine constructively inside the lens. In calculating the far field pattern, neglecting these contributions causes negligible errors since the currents relevant to multiple reflections provide incoherent field contributions. When the analysis is oriented to calculate the impedance of the antenna, the PO currents associated to the rays depicted in Fig. 2*a* must be accounted for; this leads to a further PO contribution defined as

$$\vec{J}^{PO''} = \vec{J}^{PO''}_{inc} + \vec{J}^{PO''}_{ref} = U_\Omega \hat{n} \times \vec{H}^{ref} + U_\Omega \hat{n} \times \underline{\Gamma}^{h} \cdot \vec{H}^{ref} \quad (3)$$

$$\vec{M}^{PO''} = \vec{M}^{PO''}_{inc} + \vec{M}^{PO''}_{ref} = -U_\Omega \hat{n} \times \vec{E}^{ref} - U_\Omega \hat{n} \times \underline{\Gamma}^{e} \cdot \vec{E}^{ref} \quad (4)$$

which $(\vec{E}^{ref}, \vec{H}^{ref})$ is the field of each singly reflected ray calculated at a point P of the surface A and $U_\Omega = 1$ for

$P \in A - A_\Omega$ and $U_\Omega = 0$ for $P \in A_\Omega$. Following the ray description depicted in Fig. 2*a*, for P inside A_Ω (see Fig. 2), the currents ($\vec{J}^{PO''}$, $\vec{M}^{PO''}$) are assumed to be zero.

Owing to the geometry of the lens, ray tracing does not require any minimisation of a distance function, so that the resulting algorithm is very efficient. Indeed, the specular point from which the ray-field ($\vec{E}^{ref}$, $\vec{H}^{ref}$) at a given P arises, is found by the intersection of the lens surface with a straight line passing from P to F_2.

For the same reasons as that discussed in Section 3.1, the radiation integral of the currents ($\vec{J}_{inc}^{PO''}$, $\vec{M}_{inc}^{PO''}$) is asymptotically zero inside the lens, and should be accounted for only in the external region. Indeed, the field ($\vec{E}^{ref}$, $\vec{H}^{ref}$) by which they are defined, can be regarded as that produced by a point source concentrated in the upper focus. Unlike the previous case (eqns. 1 and 2), the field radiated inside the lens by ($\vec{J}_{inc}^{PO'}$, $\vec{M}_{inc}^{PO'}$) vanishes only asymptotically and not exactly, since a first GO approximation has already been made in defining ($\vec{E}^{ref}$, $\vec{H}^{ref}$).

Finally, to predict the field scattered by the interface in the region inside the lens, the equivalent currents on A (Fig. 3) are asymptotically approximated as

$$\vec{J} = \vec{J}_{ref}^{PO'} + \vec{J}_{ref}^{PO''} \tag{5}$$

$$\vec{M} = \vec{M}_{ref}^{PO'} + \vec{M}_{ref}^{PO''} \tag{6}$$

namely, by the PO currents associated with the singly and doubly reflected rays, respectively. It should be stressed that eqns. 5 and 6 can be used only to predict the field *inside* the lens.

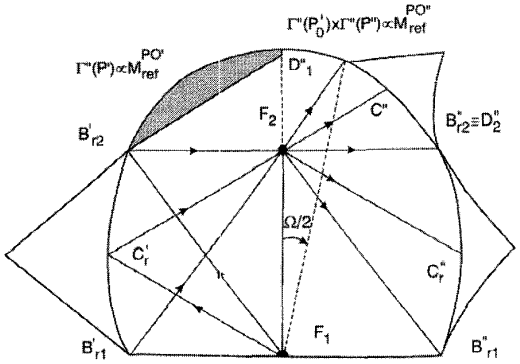

Fig. 4 *Paths of the doubly reflected rays, and profiles in the E-plane*
Left side $T''(P')$ proportional to $\vec{M}_{ref}^{PO'}$
Right side $T''(P_0') \times T''(P'')$ proporational to $\vec{M}_{ref}^{PO''}$

4 Brewster angles and near-caustic fields

Some general consideration may be given to the amplitude of the current contributions relevant to singly and doubly reflected rays. For the sake of simplicity we refer to the magnetic component $|\vec{M}_{ref}^{PO'}|$ and $|\vec{M}_{ref}^{PO''}|$ in the E-plane of the lens. At a given point P' on the lens surface, $|\vec{M}_{ref}^{PO'}|$ is proportional to the reflection coefficient for parallel polarisation $\Gamma^{\|}(P')$, and $|\vec{M}_{ref}^{PO''}|$ at P'' is proportional to $\Gamma^{\|}(P_0') \times \Gamma^{\|}(P'')$, where P_0' is the specular point from which the reflected ray impinging at P'' comes. In Fig. 4 the lens and some peculiar doubly reflected rays are depicted; also, the two curves $\Gamma^{\|}(P')$ and $\Gamma^{\|}(P_0') \times \Gamma^{\|}(P'')$ are depicted on the profile of the lens. For the sake of simplicity, the first reflection is supposed to occur on the left side of the lens and the second on the right side of the lens (as depicted in the picture). The two points C_r' and C_r'' at the end points of the minor semiaxis are illuminated under critical angle by the incident or reflected rays, respectively. For this critical angle, the maximum amplitude of both $\Gamma^{\|}(P')$ and $\Gamma^{\|}(P'')$ occurs, so that $|\vec{M}_{ref}^{PO'}|$ and $|\vec{M}_{ref}^{PO''}|$ have a maximum at C_r' and C_r'', respectively. Furthermore, $|\vec{M}_{ref}^{PO''}|$ has also a maximum at $P'' = C''$, that is illuminated by the ray coming from $P_0' = C_r'$ (maximum of $\Gamma^{\|}(P_0')$).

In the E-plane, two points B_{r1}' and B_{r2}' occur in which the incident ray impinges on the lens surface with Brewster angle. Consequently, $|\vec{M}_{ref}^{PO'}|$ exhibits nulls at B_{r1}' and B_{r2}'. By straightforward algebra it can be demonstrated that the condition $e = 1/\sqrt{\varepsilon_r}$ ensures that B_{r1}'' and B_{r2}'' are located at the same z level of the two foci F_1 and F_2, respectively. The current distribution $|\vec{M}_{ref}^{PO''}|$ vanishes at the points $P'' = B_{r1}''$ and $P'' = B_{r2}''$, where the singly reflected rays impinge again under Brewster angle on the profile on the right. Furthermore, $|\vec{M}_{ref}^{PO''}|$ vanishes at the points $P'' = D_1''$ and $P'' = D_2''$; indeed, these points are illuminated by the zero-amplitude rays that arise from $P_0' = B_{r1}$ and $P_0' = B_{r2}$. The geometrical properties ensure that D_2'' is coincident with B_{r2}'' and D_1'' located at the boundary of the shadow region A_Ω (Fig. 2*b*).

The mechanisms described above produce in general the same profile of currents in the E-plane. In particular, the presence of the Brewster points provides a change of sign in $\Gamma^{\|}(P')$. On the contrary, owing to the coincidence of D_2'' with B_{r2}'', $\Gamma^{\|}(P_0') \times \Gamma^{\|}(P'')$ exhibits a double-zero there with the consequence that it does not change sign over the entire angular range where $\vec{M}_{ref}^{PO''}$ has to be integrated. As will be shown next, this difference produces a different behaviour of the PO field contributions relevant to singly and doubly reflected rays close to the caustic points.

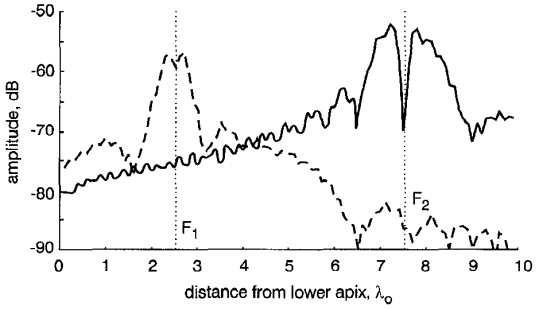

Fig. 5 *Amplitude of different magnetic field contributions on the lens axis*
($e = 0.5$, $\varepsilon_{r1} = 4$, major semiaxis = $5\lambda_0$); $|\vec{H}^{PO'} \cdot \hat{x}|$, ——— $|\vec{H}^{PO''} \cdot \hat{x}|$, – – –

Let us denote $\vec{H}^{PO'}$ and $\vec{H}^{PO''}$ the field contributions radiated by the current distributions ($\vec{J}_{ref}^{PO'}$, $\vec{M}_{ref}^{PO'}$) and ($\vec{J}_{ref}^{PO''}$, $\vec{M}_{ref}^{PO''}$), respectively. In Fig. 5, continuous and dashed lines represent $|\vec{H}^{PO'} \cdot \hat{x}|$ and $|\vec{H}^{PO''} \cdot \hat{x}|$, respectively, as a function of the z axis. A full lens (without ground plane) is considered, with eccentricity $e = 0.5$, ($\varepsilon_{r1} = 4$), and major semiaxis $5\lambda_0$ (λ_0 = free-space wavelength), which is fed by a half-wavelength resonant magnetic source oriented along $\hat{x}$. It is apparent that $|\vec{H}^{PO'} \cdot \hat{x}|$ is concentrated around the upper focus of the ellipse, where the caustic of singly reflected rays occurs. In contrast, $|\vec{H}^{PO''} \cdot \hat{x}|$ is concentrated around the feed-focus F_1 which is the point caustic of the doubly

reflected rays. At the same point F_1, $|\vec{H}^{PO'} \cdot \hat{x}|$ is negligible, due to the fact that here the PO currents relevant to singly reflected rays give incoherent contributions. This demonstrates that $|\vec{H}^{PO''} \cdot \hat{x}|$ dominates in calculating the input admittance of the antenna. It is worth noting that a local selective minimum $|\vec{H}^{PO'} \cdot \hat{x}|$ occurs at the upper focus F_2, that can be attributed to the presence of Brewster angles of the incident field. Indeed, the field contributions of $(\vec{J}_{ref}^{PO'}, \vec{M}_{ref}^{PO'})$ from portions of the ellipse above and below the Brewster point B_{r2} possess opposite signs due to the intrinsic nature of the reflection coefficients (see Fig. 4). This provides a partial cancellation of the field that produces at the caustic point a local inversion of trend in the global increase of the caustic field. This same behaviour does not occur for $|\vec{H}^{PO''} \cdot \hat{x}|$ close to F_1, since $\Gamma^{\parallel}(P_0') \times \Gamma^{\parallel}(P'')$ always possesses the same sign over the total integration domain (Fig. 4).

Fig. 6 shows the amplitude and phase of the contribution $|\vec{H}^{PO''} \cdot \hat{x}|$ when the observation point moves along the x axis (the axis that contains the slot). As expected, the field is concentrated on the slot zone. This also confirms the validity of assuming the ground plane to be infinite. Furthermore, both amplitude and phase are almost uniform along the slot.

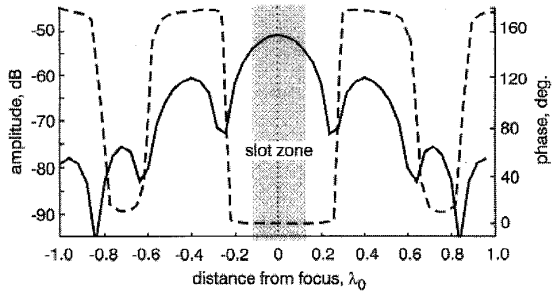

Fig. 6 *Amplitude and phase of the contribution $\vec{H}^{PO''} \cdot \hat{x}$ along the minor axis of the ellipse (parallel to the slot)*
$e = 0.5$, $\varepsilon_{r1} = 4$, major semiaxis $= 5\lambda_0$
The shadowed region corresponds to that occupied by the slot

5 Input admittance

The method discussed in the previous section allows prediction of the input admittance Y_{inp} of the antenna from

$$Y_{inp} = Y_1 + Y_2$$
$$Y_i = \iint_S (-1)^i \vec{m}(x,y) \cdot \vec{H}_i(x,y) dx dy \qquad (7)$$

where Y_i is the admittance of the magnetic source $\vec{m}(x, y)$ when radiating in the region $i = 1, 2$. In eqn. 7 S is the slot surface, and $\vec{H}_i$ is the field radiated by the magnetic source in region i. The calculation of $\vec{H}_2$ is accomplished by using the Green's function of a homogeneous grounded dielectric half-space with constant ε_{r2} The magnetic field $\vec{H}_1$ is calculated by superimposing the incident field radiated by $\vec{m}$ into a homogeneous, grounded dielectric medium of constant ε_{r1}, and the contribution $\vec{H}^{PO''}$ of the currents relevant to the doubly reflected rays. Obviously, to account for the ground plane, the image principle can be applied so that the various radiation integrals always use the Green's function of a fully homogeneous medium. Furthermore, it should be noted that the integrand of the radiation integral that defines $\vec{H}^{PO''}$ at the slot does not have relevant oscillations (owing to the presence of the caustic), so that the numerical integration does not require extensive effort even for a lens of large size in terms of a wavelength. In particular, inside the integral that define $\vec{H}^{PO''}$ a multiplying phase factor $\exp(-j4k\sqrt{\varepsilon_r}\, b)$ occurs, where b is the length of the major semiaxis. This simply derives from the fact that the total path of each doubly reflected ray is exactly $4b$, as can be deduced from simple geometrical considerations. This factor ensures the dependence of $Y^{PO''}$ on the frequency, as will be shown in the results of Fig. 7. This shows the real and imaginary part of the input admittance calculated via eqn. 6 as a function of the major semiaxis of the lens expressed in dielectric wavelengths. These results are obtained by assuming the length of the slot equal to $\lambda(2\sqrt{(\varepsilon_{r1} + \varepsilon_{r2})}/2)$; the magnetic current $\vec{m}(x, y)$ that simulates the slot has been forced to be cosinusoidal in x (with nulls at the ends) and uniform in y. Two situations have been considered in Fig. 7, corresponding to $\varepsilon_{r1} = \varepsilon_{r2} = 4$ (quartz), and $\varepsilon_{r1} = \varepsilon_{r2} = 11.7$ (silicon). Although in practical applications the dielectric constant of the lower medium is $\varepsilon_{r2} = 1$, the situations that are proposed allow illustration of the principle, while retaining simplicity. Both the conductance and the susceptance have been normalised to values that the conductance g_0 assumes at resonance for an infinite homogeneous dielectric; namely $g_0 = 0.81 \times 10^{-2}\Omega^{-1}$ ($r_0 = 1/g_0 = 123\Omega$) for $\varepsilon_{r2} = 4$ and $g_0 = 2.37 \times 10^{-2}\Omega^{-1}$ ($r_0 = 1/g_0 = 42\Omega$) for $\varepsilon_{r2} = 11.7$. It is found that the input impedance exhibits oscillations with a period of a quarter of dielectric wavelength, as expected.

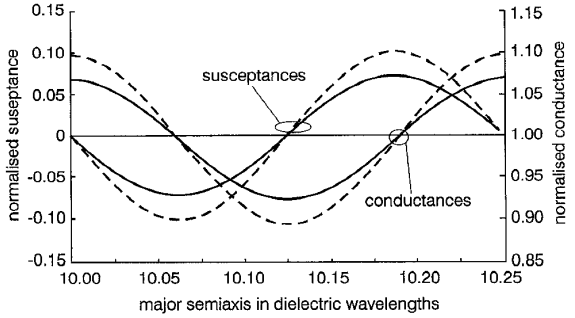

Fig. 7 *Input impedance of the slot against the major semiaxis of the lens expressed in dielectric wavelengths*
(a) Normalised resistance (b) Normalised reactance
$\varepsilon_r = 4$ – – – –
$\varepsilon_r = 11.7$ ——

6 Concluding remarks

An efficient method for calculating the field inside the dielectric lens of a millimetre wave antenna has been presented, which is based on radiation of the PO currents associated with singly and doubly reflected rays. As expected, the PO contribution of the doubly reflected ray currents is dominant in describing the input impedance, according to the geometrical evidence by which all rays emanating from a focal source exactly return to the starting point after a double reflection at the lens surface. Consequently, the perturbation of the lens on the input impedance may be non-negligible. It is worth noting also that when a quarter wavelength matching layer is used (i.e. for a silicon lens ($\varepsilon_r = 11.7$)) [1, 5], the correct design should impose a tapered pro-

file of layer thickness, which is not a straightforward matter for millimetre-wave technology. Consequently, a residual mismatch also occurs when using a matching layer. In these cases also, the method proposed here can provide a useful tool for the proper design of the input impedance in terms of both matching level and bandwidth.

The analysis performed in this paper suggests that the most important zone of the lens surface to be matched by a layer, is that located close to the maximum perimeter of the lens, where the primary rays impinge on the lens surface under critical angle (i.e. with maximum amplitude of the reflection coefficient). In contrast, the zone close to the vertex of the ellipse is associated with rays that undergo a second reflection at the ground plane and are not refocused at the primary source. Therefore, this region is not critical, at variance with what occurs in parabolic antennas, in which vertex plates are commonly used to reduce feed mismatching.

7 Acknowledgments

This work has been supported by the European Space Agency (ESA). The authors would like to thank M.J.M van der Vorst for useful discussions on this topic.

8 References

1 FILIPPOVIC, D.F., GEARHART, S.S., and REBEIZ, G.M.: 'Double slot on extended hemispherical and elliptical silicon dielectric lenses', *IEEE Trans. Microw. Theory Tech.*, 1993, **41**, (10)
2 REBEIZ, G.M.: 'Millimeter save and terahertz integrated circuit antennas', *Proc. IEEE*, 1992, **80**, (11), pp. 1748–1770
3 ADLER, C.J., BREVIT-TAYLOR, C.R., DIXON, M., HODGES, R.D., IRVING, L.D., and REES, H.D.: 'Microwave and millimeter wave receivers with integral antennas', *IEE Proc. H*, 1991, **138**, pp. 253–257
4 SKALARE, A., de GRAAUV, TH., and VAN DE STADT, H.: 'A planar dipole array antenna with an elliptical lens', *Microwave Opt. Tech. Lett.*, 1991, **4**, pp. 9–12
5 VAN DER VORST, M.J.M., DE MAAGT, P.J.I., and HERBEN, M.H.A.J.: 'Matching layers for integrated lens antennas'. International symposium on *Antennas* (JINA), Nice, France, November 1996